metals

MDPI

Article

The Effect of Ca on In Vitro Behavior of Biodegradable Zn-Fe Alloy in Simulated Physiological Environments

Orit Avior [1,*], Noa Ben Ghedalia-Peled [2], Tomer Ron [1], Razi Vago [2] and Eli Aghion [1]

[1] Department of Materials Engineering, Ben-Gurion University of the Negev, Beer-Sheva 8410501, Israel; toron@post.bgu.ac.il (T.R.); egyon@bgu.ac.il (E.A.)

[2] Department of Biotechnology Engineering, Ben-Gurion University of the Negev, Beer-Sheva 84105, Israel; noabeng@post.bgu.ac.il (N.B.G.-P.); rvago@bgu.ac.il (R.V.)

* Correspondence: oritgree@post.bgu.ac.il; Tel.: +972-542283151

Received: 11 November 2020; Accepted: 1 December 2020; Published: 3 December 2020

Abstract: The growing interest in Zn based alloys as structural materials for biodegradable implants is mainly attributed to the excellent biocompatibility of Zn and its important role in many physiological reactions. In addition, Zn based implants do not tend to produce hydrogen gas in in vivo conditions and hence do not promote the danger of gas embolism. However, Zn based implants can provoke encapsulation processes that, practically, may isolate the implant from its surrounding media, which limits its capability of performing as an acceptable biodegradable material. To overcome this problem, previous research carried out by the authors has paved the way for the development of Zn-Fe based alloys that have a relatively increased corrosion rate compared to pure Zn. The present study aims to evaluate the effect of 0.3–1.6% Ca on the in vitro behavior of Zn-Fe alloys and thus to further address the encapsulation problem. The in vitro assessment included immersion tests and electrochemical analysis in terms of open circuit potential, potentiodynamic polarization, and impedance spectroscopy in phosphate buffered saline (PBS) solution at 37 °C. The mechanical properties of the examined alloys were evaluated by tension and hardness tests while cytotoxicity properties were examined using indirect cell metabolic activity analysis. The obtained results indicated that Ca additions increased the corrosion rate of Zn-Fe alloys and in parallel increased their strength and hardness. This was mainly attributed to the formation of a Ca-rich phase in the form $CaZn_{13}$. Cytotoxicity assessment showed that the cells' metabolic activity on the tested alloys was adequate at over 90%, which was comparable to the cells' metabolic activity on an inert reference alloy Ti-6Al-4V.

Keywords: biodegradable implants; cell viability; in vitro; zinc; Zn-Fe-Ca

1. Introduction

Traditional structural materials for metallic implants in orthopedic applications such as bone plates and screws as well as stents for cardiovascular use are produced from stainless steels, Ti based alloys, Cobalt–chromium alloys, and others [1]. These implants have excellent corrosion resistance in in vivo conditions along with superior mechanical properties [2]. However, in the long run, these permanent implants may cause a variety of problems including premature failure and stress shielding [3]. Hence, an interest in developing metallic biodegradable implants made of Mg, Fe and Zn based alloys [4–7] is steadily growing. Studies related to Mg based alloys [8–19] revealed several major problems, including accelerated corrosion rates, premature degradation of mechanical integrity, and the release of hydrogen gas. The accumulation of hydrogen in in vivo conditions can produce gas bubbles that, in extreme

cases, may penetrate the bloodstream [20,21] and promote the danger of gas embolism. As for Fe based implants, their main disadvantages are limited mechanical properties and relatively reduced corrosion rates [22–25]. In addition, they produce large amounts of harmful iron oxide that repels neighboring tissue, stimulates inflammation and, in certain conditions, can be even toxic [26,27].

In the light of the inherent limitations of Mg and Fe based alloys as biodegradable implants, Zn based alloys seem to be an interesting alternative. This can be attributed to the excellent biocompatibility of Zn and its important role in many enzymatic reactions and bone metabolism. Zn is also considered to be an anti-bacterial [28] and anti-viral [29] element which is crucial for preventing inflammation in the vicinity of the implant. In addition, the degradation of Zn does not tend to produce hydrogen gas, as in the case of Mg, and hence reduces the danger of gas embolism. In spite of those relative advantages, pure Zn has a reduced corrosion rate (higher than Fe but lower than Mg) and insufficient mechanical properties [30–32]. Furthermore, pure Zn tends to provoke encapsulation processes in in vivo conditions [33], which can isolate the implant from the physiological environment and hence limits its capability to act as a suitable biodegradable material. This encapsulation problem was partly addressed in previous studies of the authors [34–36] by developing innovative Zn-Fe based alloys that have relatively increased corrosion rates compared to pure Zn. The present study aims to evaluate the effect of 0.3–1.6% Ca on in vitro behavior of Zn-Fe alloys in order to further address the encapsulation problem while maintaining adequate mechanical properties. Here, we hypothesize that the encapsulation response is regulated by the corrosion rate of the biodegradable alloy.

2. Materials and Methods

2.1. Alloys Preparation

Zn based alloys in the form of Zn-2%Fe and Zn-2%Fe with various amounts of Ca (0.3%, 0.6%, 1%, and 1.6%) were prepared by gravity casting. The selected concentration of Ca relates to the fact that this alloying element has a significant embrittlement effect on Zn based alloys and hence should be kept as low as possible. Alloy preparation was carried out in a graphite crucible using pure Zn ingots (99.99%), pure iron (99%) with powder size up to 44 microns (−325 mesh) and pure calcium in the form of granules. The alloying process was performed at 750 °C for 3 h along with active stirring every 30 min. The molten alloy was cast as bars in a rectangular steel die with the following dimensions: 6 cm × 6 cm × 15 cm. The as-cast bars were machined to obtain rods with 13 mm diameter. Later, the rods were extruded using an extrusion ratio of about 1:5. Prior to the extrusion process, the rods were preheated to 350 °C. The final dimension of the obtained rods was 6 mm. The chemical composition of the tested alloys was analyzed using an Inductively Coupled Plasma Optical Emission Spectrometer (ICP-SPECTRO, ARCOS FHS-12, Kelve, Germany) facility.

2.2. Microstructure Characterization

Microstructural examination was carried out using a JEOL JSM-5600 (JEOL, Tokyo, Japan) scanning electron microscopy (SEM) equipped with an Energy-dispersive X-ray spectroscopy (EDS) detector (Thermo Fisher Scientific, Waltham, MA, USA) for spot chemical analysis [37]. All the tested samples for SEM evaluation were polished and etched using a 5% Nital (5 mL HNO_3 + 100 mL ethanol) solution. X-ray diffraction (XRD) analysis for phase identification was carried out using an X-ray diffractometer (RIGAKU-2100H (RIGAKU, Tokyo, Japan)) with Cu-Kα. Diffraction patterns were generated between 30°–90° at 40 kV, 30 mA, and a scanning rate of 0.02°/min.

2.3. Mechanical Properties Tests

The mechanical properties of the tested alloys were evaluated in terms of tensile strength and hardness. The tensile tests were performed at room temperature using a CORMET slow strain rate machine (C76, Cormet Testing Systems, Vantaa, Finland) at a rate of 0.5 mm/min. Hardness tests were carried out by Vickers measurements using a hardness tester (Zwick/Roell Indentec (Quantarad

Technologies, Selangor, Malaysia)) with an applied load of 3 kg. Several indentations were applied to each test sample and the diagonal lengths were measured using a calibrated micrometer attached to the eyepiece of an optical microscope. The standard deviations related to tensile strength and hardness measurements were based on at least three tests for each alloy.

2.4. Immersion Test

The corrosion resistance of the tested alloys was examined by immersion tests in a simulated physiological environment in the form of a phosphate-buffered saline (PBS) solution at 37 °C. The duration of the immersion test was 14 days in line with the ASTM ID: G31-72 standard, and the pH level of the PBS solution was close to 7.4. Standard deviations were based on at least three examinations for each alloy. The corrosion products obtained after the immersion test were removed using a 10% NH_4Cl solution at 70 °C in accordance with the ASTM ID: G1-03 standard.

2.5. Electrochemical Behavior

The electrochemical behavior of the tested samples was evaluated in terms of open circuit potential, potentiodynamic polarization analysis, and impedance spectroscopy (EIS). This was carried out using a Bio-Logic SP-200 potentiostat equipped with EC-Lab software V11.18 [38]. The three-electrode cell method used for the electrochemical analysis included a saturated calomel reference electrode (SCE), a platinum counter electrode, and the tested sample as a working electrode [39,40]. The exposed area of the working electrode was 1 cm^2 and the test solution was PBS at ambient temperature. The duration of the open circuit potential tests was about 70 h in order to obtain a stable potential. The scanning rate of the potentiodynamic polarization analysis was 1 mV/s and the corrosion rates were calculated by Tafel extrapolation. The EIS measurements were performed between 10 kHz and 100 mHz at 10 mV amplitude over the open circuit potential. Prior to the electrochemical testing, the samples were cleaned in an ultrasonic bath for 5 min, washed with alcohol, and dried in hot air.

2.6. Cytotoxicity Evaluation

Indirect extract cell metabolic activity assessment was performed in order to evaluate the cytotoxicity characteristics of the tested alloys. Sample preparation and the experimental protocol were carried out in line with the ISO 10993-5/12 standard [41,42], using Mus musculus (mouse) 4T1 cells. The selection of 4T1 cells was attributed to the fact that those cells are relatively more active than primary cells and hence more sensitive to toxic insults [4]. Cylindrical samples (D = 10 mm, h = 2 mm) made from the tested Zn based alloys and a Ti-6Al-4V alloy as the reference material (control group) were prepared using four samples from each alloy. Prior to the experiment, the samples were polished up to 4000 grit, ultrasonically cleaned for 10 min in ethanol and 5 min in acetone, and then air dried followed by sterilization in ultraviolet-radiation for 1 h on each disk side. All the Zn based alloys and Ti-6Al-4V samples were pre-incubated for 24 h in Dulbecco Modified Eagle's Medium (DMEM) supplemented with 4.5 g L^{-1} D-Glucose, 10% Fetal Bovine Serum (FBS), 4 mM L-Glutamine, 1 mM Sodium Pyruvate, and 1% Penicillin Streptomycin Neomycin (PSN) antibiotic mixture at 37 °C in a humidified atmosphere. The surface area to volume extraction ratio was 1.25 cm^2 mL^{-1}. In parallel, the cells were seeded in 96-well tissue culture plates with a density of 5000 cells per well to allow substrate attachment. After 24 h, the liquids from all samples were collected and filtered by a PVDF membrane (0.45 μm), and 100 μL of metal extract was added to the cells. The negative control group contained cells cultured with only DMEM, while the positive control group contained cell cultures with 90% DMEM and 10% DMSO for toxic evaluation. Cell metabolic activity was assessed using a Cell Proliferation Kit (XTT, Biological Industry, Beit Haemek, Israel) and a microplate reader (SYNERGY-Mx, BioTek, Winooski, Vermont, USA) after 24 h and 48 h incubation at 37 °C in a 5% CO_2 humidified atmosphere. The testing process includes adding 50 μL reagent and 1 μL activator to 100 μL DMEM in each sample well for 2 h incubation. The resulting color formation was measured spectrophotometrically

at 490 nm using the microplate reader. As the cell metabolic activity is an indirect measurement of cell viability, the cell viability was calculated according to the following equation:

$$\text{Viability } (\%) = \frac{\text{OD}_{\text{Sample}}}{\text{OD}_{\text{Control}}} \times 100\% \quad (1)$$

where $\text{OD}_{\text{Sample}}$ is the optical density determined by the cells cultured with the tested extracts and $\text{OD}_{\text{Control}}$ is the optical density measurement of the cells in the control culture media [4]. Subsequent to this experiment, a pH test was performed on the medium cell (ORION PrepHec T ROSS comb. Micro pH 8220BNWP, Thermo Scientific, Waltham, Massachusetts, USA) using at least three measurements. This was followed by a visual examination of the cells was documented by a CoolLED pE-2 collimator fitted to an inverted phase-contrast microscope (Eclipse Ti, Nikon, Tokyo, Japan) that was equipped with a digital camera (DS-Qi1Mc, Nikon, Tokyo, Japan).

3. Results

The composition of the test alloys (in wt.%) obtained by optical emission spectrometer is shown in Table 1. Phase identification obtained by X-ray diffraction analysis revealed the presence of three major phases: pure Zn, a Fe-rich phase, and a Ca-rich phase, as shown in Figure 1. The Fe-rich phase was identified as $Zn_{11}Fe$ (according to ICDD 045-1184), and the Ca-rich phase was identified as $CaZn_{13}$ (according to ICDD 028-0258). The intensity of the Ca-rich phase was relatively elevated as the Ca content was increased from 0.6% to 1.6%.

Table 1. Chemical composition of tested alloys (in wt.%).

Tested alloy	Fe	Ca	Cu	Al	Mg	Pb	Zn
Pure Zn	0.020	0.002	0.001	0.000	0.000	0.002	Balance
Zn-2%Fe	1.919	0.003	0.002	0.001	0.000	0.003	Balance
Zn-2%Fe-0.3%Ca	1.820	0.297	0.002	0.001	0.000	0.002	Balance
Zn-2%Fe-0.6%Ca	1.341	0.620	0.001	0.001	0.000	0.002	Balance
Zn-2%Fe-1%Ca	1.994	1.049	0.001	0.001	0.001	0.002	Balance
Zn-2%Fe-1.6%Ca	2.260	1.621	0.002	0.001	0.001	0.002	Balance

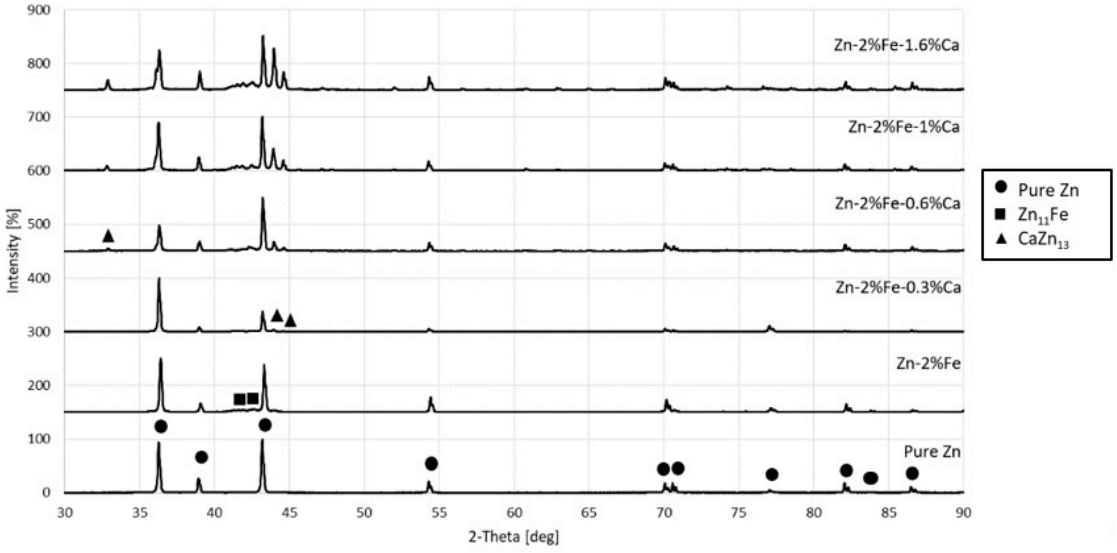

Figure 1. X-ray analysis of the tested Zn based alloys.

The typical microstructure of the examined alloys obtained by SEM is shown in Figure 2. The microstructure of the Zn-2%Fe alloy revealed a pure Zn matrix with a secondary Fe-rich phase ($Zn_{11}Fe$) that was scattered evenly across the entire bulk material, as shown in Figure 2a. In the cases of

the ternary alloys with Ca additions, the microstructure was composed of a pure Zn matrix, a Fe-rich phase, and a Ca-rich phase ($CaZn_{13}$). The dimensions and structure of the Ca-rich phase varied as the Ca content was increased. At a lower Ca content (0.6%), the Ca-rich phase was relatively fine, while, at a higher content (1.6%), this phase was significantly enlarged with a massive bulky appearance.

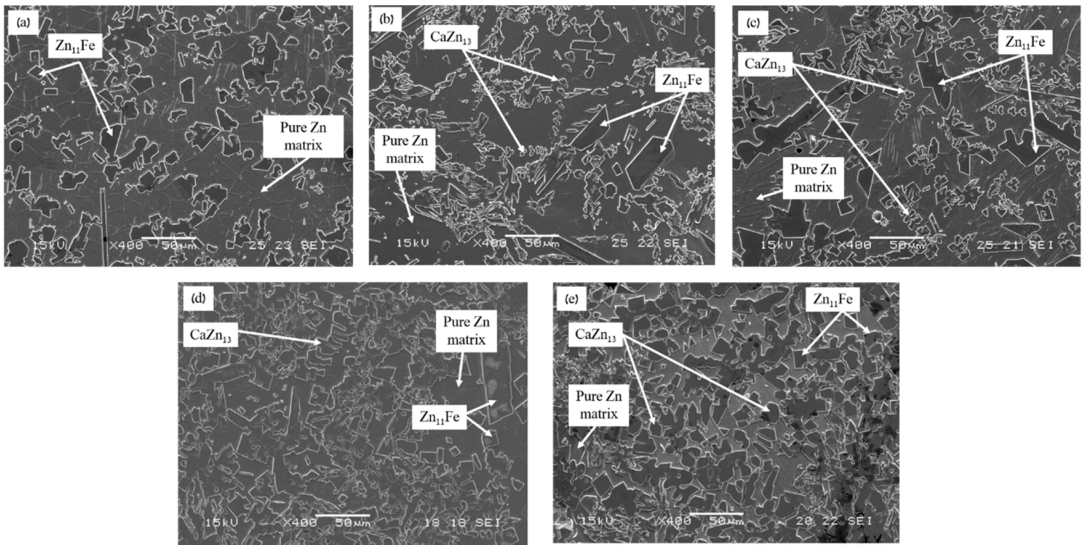

Figure 2. Typical microstructure of the tested alloys (**a**) Zn-2%Fe; (**b**) Zn-2%Fe-0.3%Ca; (**c**) Zn-2%Fe-0.6%Ca; (**d**) Zn-2%Fe-1%Ca; (**e**) Zn-2%Fe-1.6%Ca.

The embrittlement effect caused by the additions of Ca to the base alloy Zn-2%Fe is clearly illustrated by the results of the hardness and tensile tests shown in Figures 3 and 4, respectively. The significantly increased hardness as the Ca content was increased has limited the possibility of practically extruding the tested alloys (at an extrusion ratio of 1:5) when the Ca content was above 0.6%. The results of the tensile tests related to Zn-2%Fe and Zn-2%Fe-0.6%Ca alloys are summarized in Table 2. This reveals that the addition of 0.6%Ca significantly reduces the elongation of the base alloy (from 13.8% to 7.7%), while having a relatively minor deteriorating effect on the tensile strength (UTS) and yield point (YP).

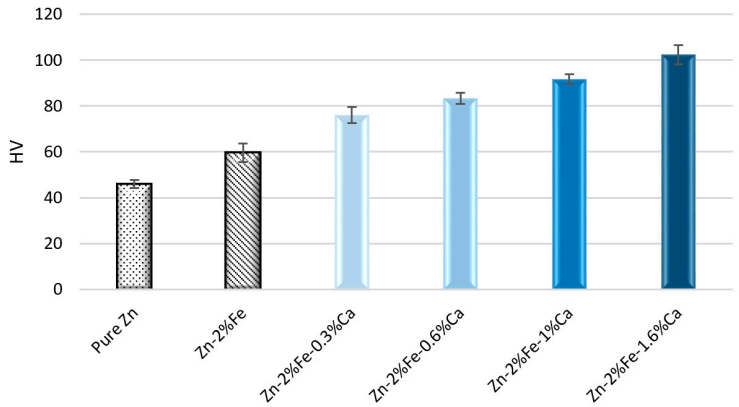

Figure 3. Hardness measurements in terms of Vickers (applied load 3 Kg).

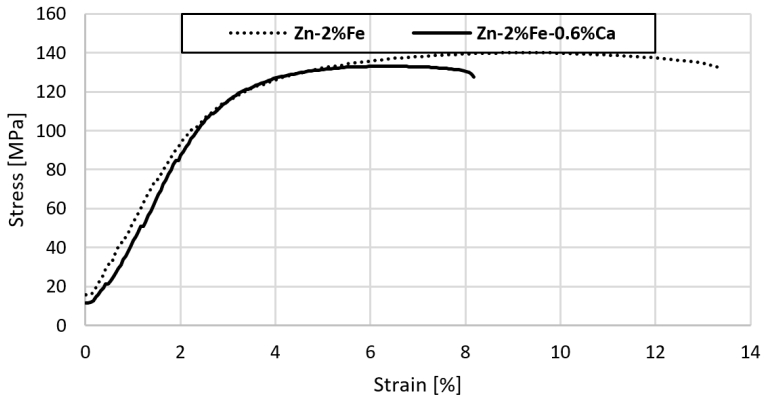

Figure 4. Stress–strain curves of base alloy Zn-2%Fe and Zn-2%Fe-0.6%Ca alloy.

Table 2. Mechanical properties of Zn-2%Fe and Zn-2%Fe-0.6%Ca alloys as obtained from the tensile tests.

Tested alloy	UTS (MPa)	YP (MPa)	Elongation (%)
Zn-2%Fe	140.3 ± 3.39	117.3 ± 6.11	13.8 ± 1.96
Zn-2%Fe-0.6%Ca	135.8 ± 2.71	112.0 ± 4.0	7.7 ± 0.46

The corrosion rate of the tested alloys obtained by immersion tests in PBS solution at a temperature of 37 °C after 14 days is shown in Figure 5. This reveals that the corrosion rate of the base alloy tends to increase due to the additions of Ca. However, the corrosion rates of the alloys containing 0.6–1.6% Ca were relatively similar.

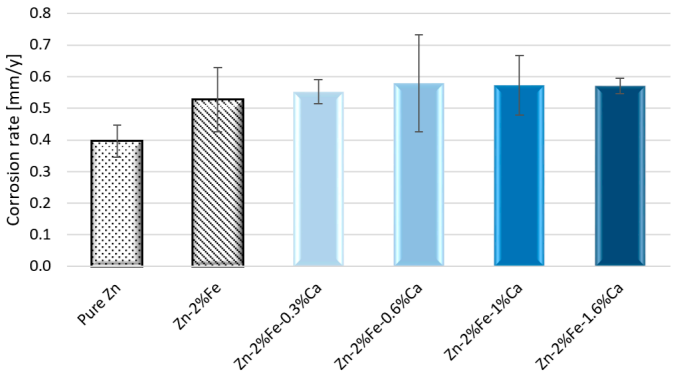

Figure 5. Corrosion rate measurements of tested alloys after immersion test in PBS solution at 37 °C for 14 days.

Electrochemical analysis in terms of open circuit potential E_{OC} is shown in Figure 6. The E_{OC} of all the tested alloys was within a narrow range between −1.03 V and −1.1 V. In addition, it was evident that, after reaching steady state conditions (beyond 50 h of exposure), the potential of the base alloy Zn-2%Fe was relatively elevated. The spike of the potential of Zn-2%Fe just before 10 h can be related to some types of contamination. Altogether, the obtained open circuit potential result comes in line with the outcome of the immersion tests that indicate that the additions of Ca increase the corrosion degradation of the base alloy.

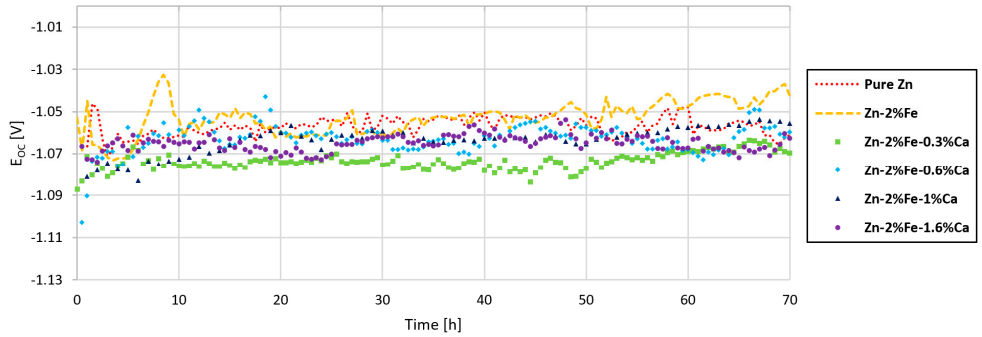

Figure 6. Open circuit potential of tested alloys in PBS solution at 37 °C.

Potentiodynamic polarization curves of the tested alloys are shown in Figure 7. This reveals that the polarization curves of the alloys containing Ca were shifted to relatively higher current densities compared to the base alloy Zn-2%Fe. This can be an indication of relatively higher corrosion degradation characteristics of the alloys containing Ca. This assumption was supported by Tafel extrapolation analysis in terms of corrosion potentials (E_{CORR}), corrosion current densities (I_{CORR}), and corrosion rates, as shown in Table 3. According to the Tafel extrapolation results, the current densities and consequent corrosion rates of the alloys containing Ca were relatively increased compared to base alloy. This again indicates that the addition of Ca clearly reduces the corrosion resistance of the base alloy.

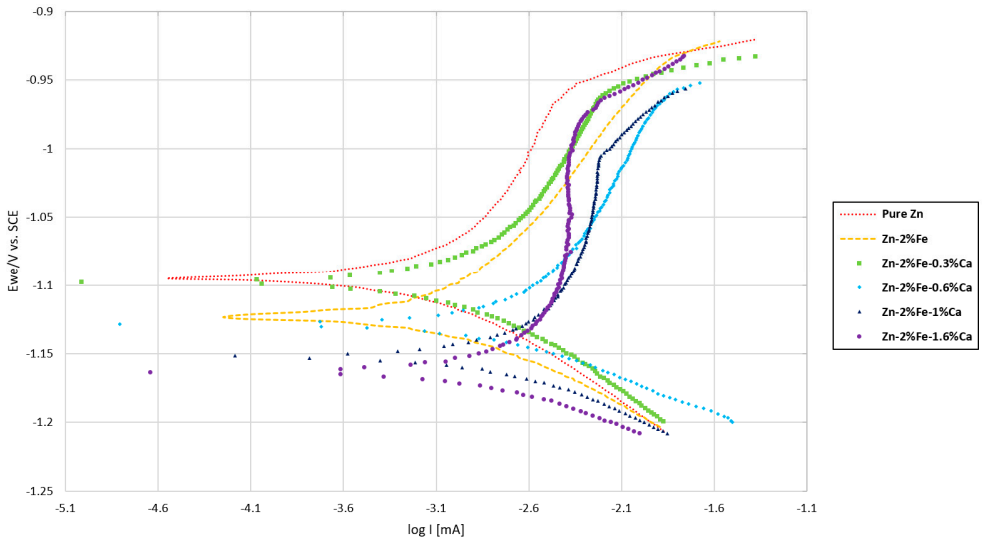

Figure 7. Potentiodynamic polarization analysis of the tested alloys in PBS solution.

Table 3. Tafel extrapolation measurement obtained from the potentiodynamic polarization analysis.

Corrosion Parameter	Pure Zn	Zn-2%Fe	Zn-2%Fe-0.3%Ca	Zn-2%Fe-0.6%Ca	Zn-2%Fe-1%Ca	Zn-2%Fe-1.6%Ca
E_{CORR} [V]	−1.0943	−1.1233	−1.0978	−1.1287	−1.1515	−1.1657
I_{CORR} [uA]	0.115	0.118	0.201	0.41	0.509	0.596
Corrosion rate [mmpy]	0.0017	0.0018	0.0030	0.0062	0.0076	0.0089

The corrosion degradation kinetics of the tested alloys were further analyzed by impedance spectroscopy (EIS), as shown in Figure 8. The Nyquist plots reveal that the radii of curvature of the alloys containing Ca were relatively reduced compared to that of the base alloy Zn-2%Fe. This indicates that the corrosion resistance of the alloys containing Ca was relatively reduced. This outcome was

also supported by the Bode curves that clearly illustrate the differences between the base alloy and the alloys containing Ca. In order to provide detailed information relating to the corrosion process at the electrolyte/electrode interface, electrical equivalent circuit (EEC) fitting was generated based on the Nyquist plots. The EECs fitted to model the EIS spectra are shown in Figure 9, while the relevant outcomes are reported in Table 4. The fitted EEC had the lowest chi-square values and minimum overall errors. The R_S is the solution resistance, R_{dl} is the charge transfer resistance attributed to the electrochemical reaction, and Q_{dl} is a component related to the capacitance of the double layer. Q_{dl} is a constant phase element that is governed by the exponent a, where a = 1 indicates an ideal capacitor C. As shown, the solution resistance of all tested samples was equal, and the double layer capacitance has nearly the same order of magnitude.

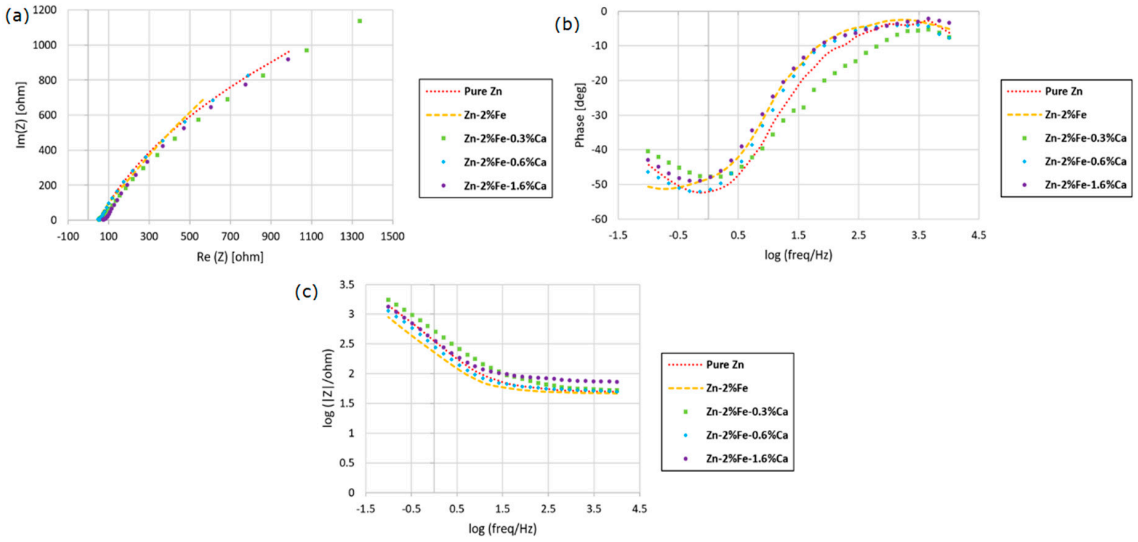

Figure 8. EIS analysis results in terms of Nyquist and Bode plots in PBS solution (**a**) Nyquist diagram; (**b**) Bode phase diagram; (**c**) Bode magnitude diagram.

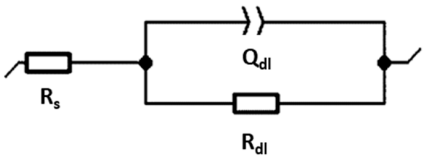

Figure 9. Electrical equivalent circuit (EEC) fitted to the Nyquist plots.

Table 4. Electrical equivalent circuit components values fitted from the Nyquist plots.

Electrical Parameter	Pure Zn	Zn-2%Fe	Zn-2%Fe-0.3%Ca	Zn-2%Fe-0.6%Ca	Zn-2%Fe-1%Ca	Zn-2%Fe-1.6%Ca
R_S [$\Omega \cdot cm^{-2}$]	50.28	47.31	52.67	52.42	53.11	76.55
Q_{dl} [$F \cdot cm^{-2} \cdot S^{(a-1)}$]	8.288×10^{-4}	14.28×10^{-4}	6.466×10^{-4}	10.25×10^{-4}	9.123×10^{-4}	8.681×10^{-4}
a	0.6937	0.6783	0.6047	0.702	0.734	0.6799
R_{dl} [$\Omega \cdot cm^{-2}$]	4198	4747	6911	3791	6044	4258

The cytotoxicity of the tested alloys was evaluated by indirect testing in terms of cells viability using a Ti-6%Al-4%V reference, as shown in Figure 10. As indicated by ISO 10993-5 [41], cell viability reduction of higher than 30% is considered to indicate a cytotoxic effect. The obtained results clearly demonstrated that the viability values of all the tested alloys were between 90–116%. Hence, it can be assumed that all the tested alloys can be non-cytotoxic substances regarding 4T1 cells. This assessment was also supported by microscopy analysis of the cells, as shown in Figure 11. According to the obtained images, the general appearance of the cells on all the tested alloys was normal and healthy

and their density was quite adequate and comparable with the cells' viability on the Ti-6%Al-4%V alloy. In addition, pH measurements of extracted media post incubation of 4T1 cells on all the Zn based alloys were very similar to the measurement obtained by the reference Ti-6%Al-4%V alloy, as shown in Figure 12. It should be pointed out that independent cytotoxicity tests were carried out twice with very similar outcomes.

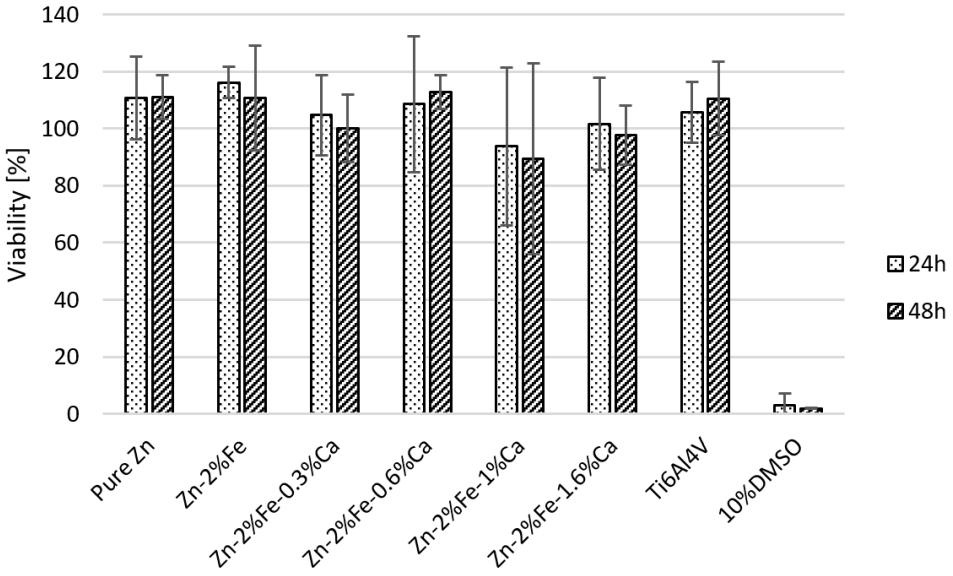

Figure 10. Quantitative analysis of 4T1 cell metabolic activity in extracted media obtained from the tested alloys after 24 and 48 h of incubation.

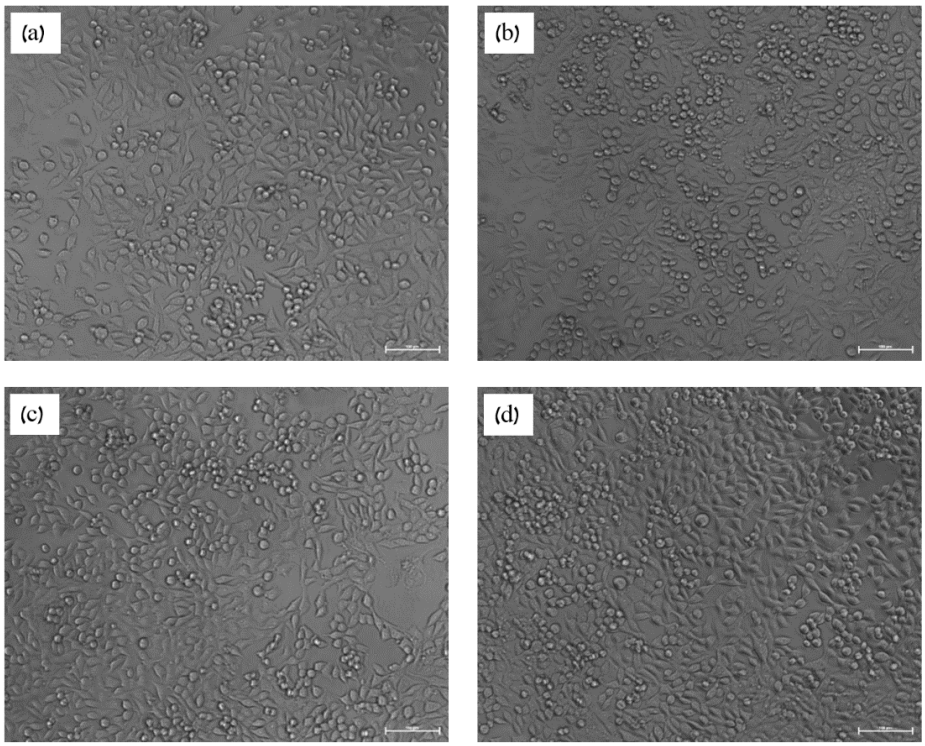

Figure 11. *Cont.*

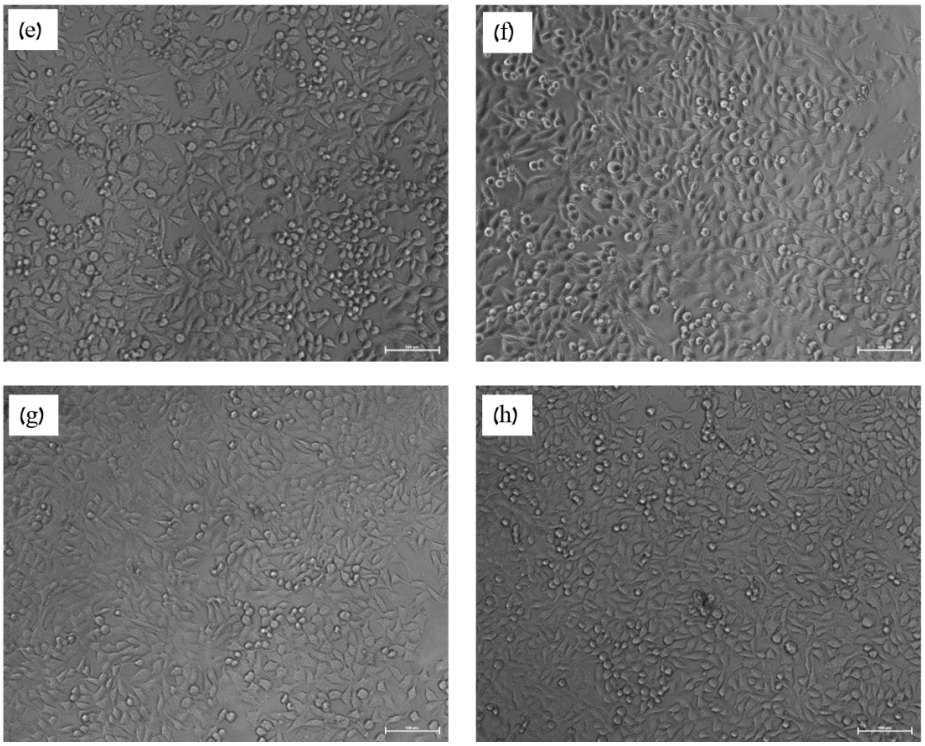

Figure 11. The general appearance of 4T1 cells after 24 h of incubation within the 48 h incubated extract media of the tested alloys of (**a**) Pure Zn; (**b**) Zn-2%Fe; (**c**) Zn-2%Fe-0.3%Ca; (**d**) Zn-2%Fe-0.6%Ca; (**e**) Zn-2%Fe-1%Ca; (**f**) Zn-2%Fe-1.6%Ca; (**g**) Ti-6Al-4V; (**h**) DMEM only.

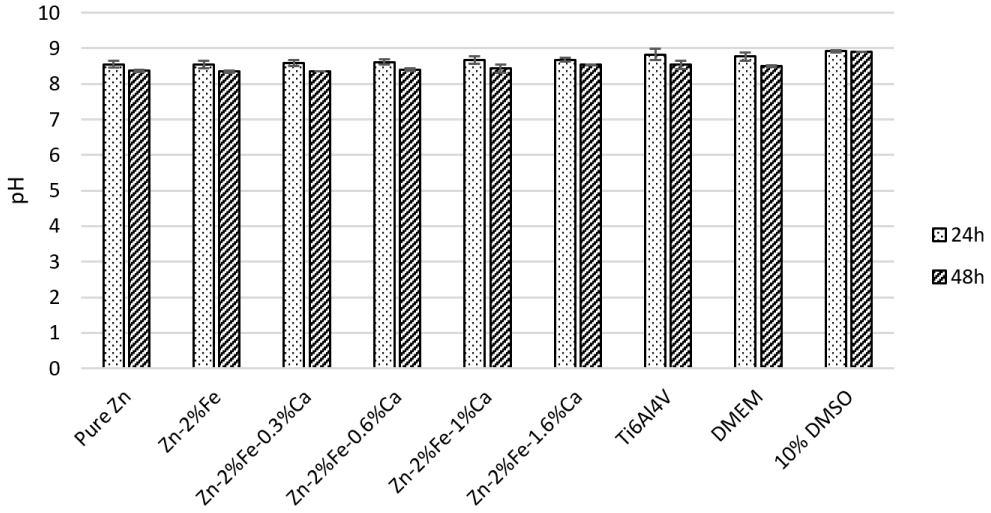

Figure 12. pH measurements of extracted media post incubation of 4T1 cells.

4. Discussion

The present study addresses the inherent disadvantage of Zn in terms of its biodegradation characteristics in physiological environments. This disadvantage mainly relates to the relatively elevated potential of Zn (−0.76 V) compared, for example, to Mg (−2.37 V) [43]. Consequently, according to Guillory et al. [33], pure Zn and Zn based alloys tend to provoke inflammation and fibrous encapsulation. The encapsulation event can practically isolate the implant from the surrounding physiological environment, and subsequently limits its capability to perform as a biodegradable material [44,45]. In order to address this problem, previous research activities carried out by the authors [34,36,46] paved the way for the development of Zn-Fe based alloys that have a relatively

increased corrosion rate compared to pure Zn. The additions of various amounts of Ca with a relatively lower potential (−2.87 V) to Zn-Fe based alloys aim to further increase the degradation rate of those alloys in order to overcome the problem of encapsulation.

The results obtained by this study in terms of immersion test and electrochemical analysis (open circuit potential, potentiodynamic polarization, and impedance spectroscopy) clearly indicate that additions of 0.3–1.6 Ca increase the corrosion rate of the base Zn-2%Fe alloy. This was mainly attributed to the formation of a Ca-rich phase in the form of $CaZn_{13}$ that, according to Li et al. [47], increases the corrosion of pure Zn, probably due to a micro-galvanic effect. The selected amount of Ca (0.3–1.6%) was related to the processing capabilities of the tested alloys in terms of the extrusion process as well as due to the fact that this element is considered an essential bone constituent and one of the vital elements in human body [48]. It was evident that alloys containing more than 0.6%Ca could not be practically extruded at a suitable extrusion ratio of 1:5. This can be related to the hardening effect of $CaZn_{13}$ phase, as clearly indicated by the hardness and tensile tests. This assumption was also supported by Shi et.al [49], who showed that the hardness of the $CaZn_{13}$ phase was three times higher than for pure Zn. In addition, the FCC structure of the $CaZn_{13}$ phase, with a primary growth direction of <111> and a secondary favorable direction <010>, had a morphology of a fine three-petaled flower [49] at a lower Ca content (up to 0.6%), while with higher amounts of Ca this phase was significantly enlarged with a massive bulky appearance. Hence, the inherent embrittlement effect of the $CaZn_{13}$ phase in alloys containing more than 0.6% Ca was due to the increased amount of that phase and morphology transformation.

Relating to the cytotoxicity characteristics of the tested alloys in terms of indirect cell metabolic activity analysis, it was evident that the tested alloys showed over 90% cell viability, which was comparable to the cell viability obtained by the reference Ti-6Al-4V alloy. Hence, according to this result, it can be concluded that the additions of Ca to the base Zn-2%Fe did not impair the adequate biocompatibility characteristics of this alloy. It should be pointed out that the selection of 4T1 cells for the cytotoxicity analysis was related to the fact that these cells are relatively much more active than primary cells and consequently more sensitive to toxic insults [4]. In addition, as the outcome of this study relates only to in vitro analysis, additional evaluation in in vivo conditions is required in order for the prospects of Zn-Fe-Ca based alloy as structural materials for biodegradable implants can be practically realized.

5. Conclusions

The obtained results showed that additions of 0.3–1.6% Ca to Zn-2%Fe alloy increased the corrosion rate of this alloy and hence subsequently reduced the possible risk of encapsulation. It is believed that this was mainly attributed to the formation of a $CaZn_{13}$ phase that creates a detrimental micro-galvanic effect. The processing capabilities of the alloys with Ca in terms of an extrusion process indicate that alloys containing more than 0.6%Ca could not be extruded at a suitable extrusion ratio of 1:5. This was mainly related to the hardening effect of the $CaZn_{13}$ phase. Cytotoxicity analysis in terms of indirect cell viability on Zn-2%Fe alloys containing Ca was adequate and comparable to the cells' viability on a reference Ti-6Al-4V alloy. This indicates that the alloys with Ca can be considered to have acceptable biocompatibility characteristics.

Author Contributions: Designed the experiments and wrote the paper: E.A. and O.A.; performed the experiments: O.A.; assisted with the experiments: T.R.; assisted with the experiments relating to cytotoxicity evaluation: N.B.G.-P. and R.V. All authors have read and agreed to the published version of the manuscript.

Funding: This research received no external funding.

Conflicts of Interest: The authors declare no conflict of interest.

References

1. Chen, Q.; Thouas, G.A. Metallic implant biomaterials. *Mater. Sci. Eng. R: Rep.* **2015**, *87*, 1–57. [CrossRef]
2. Niinomi, M.; Nakai, M.; Hieda, J. Development of new metallic alloys for biomedical applications. *Acta Biomater.* **2012**, *8*, 3888–3903. [CrossRef] [PubMed]
3. Aksakal, B.; Yildirim, Ö.S.; Gul, H. Metallurgical failure analysis of various implant materials used in orthopedic applications. *J. Fail. Anal. Prev.* **2004**, *4*, 17–23. [CrossRef]
4. Levy, G.K.; Leon, A.; Kafri, A.; Ventura, Y.; Drelich, J.W.; Goldman, J.; Vago, R.; Aghion, E. Evaluation of biodegradable Zn-1%Mg and Zn-1%Mg-0.5%Ca alloys for biomedical applications. *J. Mater. Sci. Mater. Med.* **2017**, *28*, 174. [CrossRef] [PubMed]
5. Hakimi, O.; Aghion, E.; Goldman, J. Improved stress corrosion cracking resistance of a novel biodegradable EW62 magnesium alloy by rapid solidification, in simulated electrolytes. *Mater. Sci. Eng. C* **2015**, *51*, 226–232. [CrossRef]
6. Dunne, C.F.; Levy, G.K.; Hakimi, O.; Aghion, E.; Twomey, B.; Stanton, K.T. Corrosion behaviour of biodegradable magnesium alloys with hydroxyapatite coatings. *Surf. Coatings Technol.* **2016**, *289*, 37–44. [CrossRef]
7. Aghion, E.; Yered, T.; Perez, Y.; Gueta, Y. The Prospects of Carrying and Releasing Drugs via Biodegradable Magnesium Foam. *Adv. Eng. Mater.* **2010**, *12*, B374–B379. [CrossRef]
8. Feyerabend, F. The history of biodegradable magnesium implants: A review. *Acta Biomater.* **2010**, *6*, 1680–1692. [CrossRef]
9. Persaud-Sharma, D.; McGoron, A. Biodegradable Magnesium Alloys: A Review of Material Development and Applications. *J. Biomim. Biomater. Tissue Eng.* **2012**, *12*, 25–39. [CrossRef]
10. Esmaily, M.; Svensson, J.; Fajardo, S.; Birbilis, N.; Frankel, G.; Virtanen, S.; Arrabal, R.; Thomas, S.; Johansson, L. Fundamentals and advances in magnesium alloy corrosion. *Prog. Mater. Sci.* **2017**, *89*, 92–193. [CrossRef]
11. Aghion, E.; Gueta, Y.; Moscovitch, N.; Bronfin, B. Effect of yttrium additions on the properties of grain-refined Mg–3%Nd alloy. *J. Mater. Sci.* **2008**, *43*, 4870–4875. [CrossRef]
12. Aghion, E.; Bronfin, B.; Eliezer, D.; Von Buch, F.; Schumann, S.; Friedrich, H.E. The Art of Developing New Magnesium Alloys for High Temperature Applications. *Mater. Sci. Forum* **2003**, *419*, 407–418. [CrossRef]
13. Regev, M.; Aghion, E.; Berger, S.; Bamberger, M.; Rosen, A. Dislocation analysis of crept AZ 91 D ingot castings. *Mater. Sci. Eng. A* **1998**, *257*, 349–352.
14. Hänzi, A.C.; Gerber, I.; Schinhammer, M.; Löffler, J.F.; Uggowitzer, P.J. On the in vitro and in vivo degradation performance and biological response of new biodegradable Mg–Y–Zn alloys. *Acta Biomater.* **2010**, *6*, 1824–1833. [CrossRef]
15. Cha, P.-R.; Han, H.-S.; Yang, G.-F.; Kim, Y.-C.; Hong, K.-H.; Lee, S.-C.; Jung, J.-Y.; Ahn, J.-P.; Kim, Y.-Y.; Cho, S.-Y.; et al. Biodegradability engineering of biodegradable Mg alloys: Tailoring the electrochemical properties and microstructure of constituent phases. *Sci. Rep.* **2013**, *3*, srep02367. [CrossRef]
16. Tie, D.; Feyerabend, F.; Müller, W.-D.; Schade, R.; Liefeith, K.; Kainer, K.U.; Willumeit, R. Antibacterial biodegradable Mg-Ag alloys. *Eur. Cells Mater.* **2013**, *25*, 284–298. [CrossRef]
17. Manivasagam, G.; Suwas, S. Biodegradable Mg and Mg based alloys for biomedical implants. *Mater. Sci. Technol.* **2014**, *30*, 515–520. [CrossRef]
18. Hopkins, T.M.; Little, K.J.; Vennemeyer, J.J.; Triozzi, J.L.; Turgeon, M.K.; Heilman, A.M.; Minteer, D.; Marra, K.; Hom, D.B.; Pixley, S. Short and long gap peripheral nerve repair with magnesium metal filaments. *J. Biomed. Mater. Res. Part A* **2017**, *105*, 3148–3158. [CrossRef]
19. Maier, P.; Hort, N. Magnesium Alloys for Biomedical Applications. *Metals* **2020**, *10*, 1328. [CrossRef]
20. Cho, S.Y.; Chae, S.-W.; Choi, K.W.; Seok, H.K.; Kim, Y.C.; Jung, J.Y.; Yang, S.J.; Kwon, G.J.; Kim, J.T.; Assad, M. Biocompatibility and strength retention of biodegradable Mg-Ca-Zn alloy bone implants. *J. Biomed. Mater. Res. Part B Appl. Biomater.* **2013**, *101*, 201–212. [CrossRef]
21. Uddin, M.S.; Hall, C.; Murphy, P.J. Surface treatments for controlling corrosion rate of biodegradable Mg and Mg-based alloy implants. *Sci. Technol. Adv. Mater.* **2015**, *16*, 053501. [CrossRef] [PubMed]
22. Montani, M.; Demir, A.G.; Mostaed, E.; Vedani, M.; Previtali, B. Processability of pure Zn and pure Fe by SLM for biodegradable metallic implant manufacturing. *Rapid Prototyp. J.* **2017**, *23*, 514–523. [CrossRef]
23. Moravej, M.; Mantovani, D. Biodegradable Metals for Cardiovascular Stent Application: Interests and New Opportunities. *Int. J. Mol. Sci.* **2011**, *12*, 4250–4270. [CrossRef] [PubMed]

24. Feng, Q.; Zhang, D.; Xin, C.; Liu, X.; Lin, W.; Zhang, W.; Chen, S.; Sun, K. Characterization and in vivo evaluation of a bio-corrodible nitrided iron stent. *J. Mater. Sci. Mater. Med.* **2012**, *24*, 713–724. [CrossRef] [PubMed]
25. Kraus, T.; Moszner, F.; Fischerauer, S.; Fiedler, M.; Martinelli, E.; Eichler, J.; Witte, F.; Willbold, E.; Schinhammer, M.; Meischel, M.; et al. Biodegradable Fe-based alloys for use in osteosynthesis: Outcome of an in vivo study after 52weeks. *Acta Biomater.* **2014**, *10*, 3346–3353. [CrossRef] [PubMed]
26. Schinhammer, M.; Gerber, I.; Hänzi, A.C.; Uggowitzer, P.J. On the cytocompatibility of biodegradable Fe-based alloys. *Mater. Sci. Eng. C* **2013**, *33*, 782–789. [CrossRef]
27. Chen, H.; Zhang, E.; Yang, K. Microstructure, corrosion properties and bio-compatibility of calcium zinc phosphate coating on pure iron for biomedical application. *Mater. Sci. Eng. C* **2014**, *34*, 201–206. [CrossRef]
28. Thian, E.S.; Konishi, T.; Kawanobe, Y.; Lim, P.N.; Choong, C.; Ho, B.; Aizawa, M. Zinc-substituted hydroxyapatite: A biomaterial with enhanced bioactivity and antibacterial properties. *J. Mater. Sci. Mater. Med.* **2013**, *24*, 437–445. [CrossRef]
29. Wei, Z.; Burwinkel, M.; Palissa, C.; Ephraim, E.; Schmidt, M.F. Antiviral activity of zinc salts against transmissible gastroenteritis virus in vitro. *Veter Microbiol.* **2012**, *160*, 468–472. [CrossRef]
30. Yang, H.; Jia, B.; Zhang, Z.; Qu, X.; Li, G.-N.; Lin, W.; Zhu, D.; Dai, K.; Zheng, Y. Alloying design of biodegradable zinc as promising bone implants for load-bearing applications. *Nat. Commun.* **2020**, *11*, 1–16. [CrossRef]
31. Tang, Z.; Niu, J.; Huang, H.; Zhang, H.; Pei, J.; Ou, J.; Yuan, G. Potential biodegradable Zn-Cu binary alloys developed for cardiovascular implant applications. *J. Mech. Behav. Biomed. Mater.* **2017**, *72*, 182–191. [CrossRef] [PubMed]
32. Levy, G.K.; Goldman, J.; Aghion, E. The Prospects of Zinc as a Structural Material for Biodegradable Implants—A Review Paper. *Metals* **2017**, *7*, 402. [CrossRef]
33. Guillory, R.J.; Bowen, P.K.; Hopkins, S.P.; Shearier, E.R.; Earley, E.J.; Gillette, A.A.; Aghion, E.; Bocks, M.L.; Drelich, J.W.; Goldman, J. Corrosion Characteristics Dictate the Long-Term Inflammatory Profile of Degradable Zinc Arterial Implants. *ACS Biomater. Sci. Eng.* **2016**, *2*, 2355–2364. [CrossRef]
34. Kafri, A.; Ovadia, S.; Yosafovich-Doitch, G.; Aghion, E. In vivo performances of pure Zn and Zn-Fe alloy as biodegradable implants. *J. Mater. Sci. Mater. Med.* **2018**, *29*, 94. [CrossRef] [PubMed]
35. Shadanbaz, S.; Dias, G.J. Calcium phosphate coatings on magnesium alloys for biomedical applications: A review. *Acta Biomater.* **2012**, *8*, 20–30. [CrossRef] [PubMed]
36. Kafri, A.; Ovadia, S.; Yosafovich-Doitch, G.; Aghion, E. The Effects of 4%Fe on the Performance of Pure Zinc as Biodegradable Implant Material. *Ann. Biomed. Eng.* **2019**, *47*, 1400–1408. [CrossRef]
37. Kaya, A.; Uzan, P.; Eliezer, D.; Aghion, E. Electron microscopical investigation of as cast AZ91D alloy. *Mater. Sci. Technol.* **2000**, *16*, 1001–1006. [CrossRef]
38. Leon, A.; Shirizly, A.; Aghion, E. Corrosion Behavior of AlSi10Mg Alloy Produced by Additive Manufacturing (AM) vs. Its Counterpart Gravity Cast Alloy. *Metals* **2016**, *6*, 148. [CrossRef]
39. Itzhak, D.; Aghion, E. Corrosion behaviour of hot-pressed austenitic stainless steel in H2SO4 solutions at room temperature. *Corros. Sci.* **1983**, *23*, 1085–1094. [CrossRef]
40. Itzhak, D.; Aghion, E. An anodic behaviour study of an analogical sintered system of austenitic stainless steel in H2SO4 solution. *Corros. Sci.* **1984**, *24*, 145–149. [CrossRef]
41. ISO-10993-5. Biological Evaluation of Medical Devices, Part 5: Tests for in Vitro Cytotoxicity. International Organization for Standardization; ISO Central Secretaria. 2009. Available online: https://www.iso.org/standard/36406.html (accessed on 3 December 2020).
42. ISO-10993-12. Biological Evaluation of Medical Devices, Part 12: Sample Preparation and Reference Materials; International Organization for Standardization, ISO Central Secretaria. 2012. Available online: https://www.iso.org/standard/53468.html (accessed on 3 December 2020).
43. Liu, Y.; Zheng, Y.; Chen, X.; Yang, J.; Pan, H.; Chen, D.; Wang, L.; Zhang, J.; Zhu, D.; Wu, S.; et al. Fundamental Theory of Biodegradable Metals—Definition, Criteria, and Design. *Adv. Funct. Mater.* **2019**, *29*, 1805402. [CrossRef]
44. Tjellström, A.; Rosenhall, U.; Lindström, J.; Hallen, O.; Albrektsson, T.; Brånemark, P.I. Five-year experience with skin-penetrating bone-anchored implants in the temporal bone. *Acta Otolaryngol.* **1983**, *95*, 568–575. [CrossRef]

45. Yue, R.; Huang, H.; Ke, G.; Zhang, H.; Pei, J.; Xue, G.; Yuan, G. Microstructure, mechanical properties and in vitro degradation behavior of novel Zn-Cu-Fe alloys. *Mater. Charact.* **2017**, *134*, 114–122. [CrossRef]
46. Kafri, A.; Ovadia, S.; Goldman, J.; Drelich, J.W.; Aghion, E. The Suitability of Zn-1.3%Fe Alloy as a Biodegradable Implant Material. *Metals* **2018**, *8*, 153. [CrossRef]
47. Li, H.F.; Xie, X.H.; Zheng, Y.; Cong, Y.; Zhou, F.Y.; Qiu, K.J.; Wang, X.; Chen, S.H.; Huang, L.; Tian, L.; et al. Development of biodegradable Zn-1X binary alloys with nutrient alloying elements Mg, Ca and Sr. *Sci. Rep.* **2015**, *5*, srep10719. [CrossRef] [PubMed]
48. Kwok, S.C.H.; Ha, P.C.T.; McKenzie, D.R.; Bilek, M.M.M.; Chu, P.K. Biocompatibility of calcium and phosphorus doped diamond-like carbon thin films synthesized by pla sma immersion ion implantation and deposition. *Diamond Relat. Mater.* **2006**, *15*, 893–897. [CrossRef]
49. Shi, Z.-Z.; Li, H.-Y.; Xu, J.-Y.; Gao, X.-X.; Liu, X.-F. Microstructure evolution of a high-strength low-alloy Zn-Mn-Ca alloy through casting, hot extrusion and warm caliber rolling. *Mater. Sci. Eng. A* **2020**, *771*, 138626. [CrossRef]